Isotactic Polypropylene/Polystyrene Blends: Effects of the Addition of a Graft Copolymer of Propylene with Styrene

L. D'ORAZIO,[1] R. GUARINO,[1] C. MANCARELLA,[1] E. MARTUSCELLI,[1] G. CECCHIN[2]

[1] Istituto di Ricerca e Tecnologia delle Materie Plastiche del CNR, Via Toiano, 6-80072 Arco Felice-Napoli, Italy

[2] Montell, Ferrara-Italy

Received 16 July 1996; accepted 18 September 1996

ABSTRACT: A novel graft copolymer of unsaturated propylene with styrene (uPP-*g*-PS) was added to binary blends of isotactic polypropylene (iPP) and atactic polystyrene (aPS) with a view to using such a copolymer as compatibilizer for iPP/aPS materials. Differential scanning calorimetry, optical microscopy, scanning electron microscopy (SEM), wide angle X-ray scattering, and small angle X-ray scattering (SAXS) techniques have been carried out to investigate the phase morphology and structure developed in solution-cast samples of iPP/aPS/uPP-*g*-PS ternary blends. It was found that the uPP-*g*-PS addition can provide iPP/aPS-compatibilized materials and that the extent of the achieved compatibilization is composition-dependent. Blends of iPP and aPS exhibited a coarse domain morphology that is characteristic of immiscible polymer systems. By adding 2% (wt/wt) of uPP-*g*-PS copolymer a very broad particle-size distribution was obtained, even though the particles appeared coated by a smooth interfacial layer, as expected according to a core–shell interfacial model. With increasing uPP-*g*-PS content (5% wt/wt), a finer dispersion degree of particles, together with morphological evidence of interfacial adhesion, was found. With further increase of uPP-*g*-PS amount (10% wt/wt) the material showed such a homogeneous texture that neither domains of dispersed phase nor holes could be clearly detected by SEM. The type of interface developed in such iPP/aPS/uPP-*g*-PS blends was accounted for by an interfacial interpenetration model. The iPP crystalline texture, size, neatness, and regularity of iPP spherulites crystallized from iPP/aPS/uPP-*g*-PS blends were found to decrease when the copolymer content was slightly increased. Assuming, for the iPP spherulite fibrillae, a two-phase model constituted by alternating parallel crystalline lamellae and amorphous layers, it was shown by SAXS that the phase structure generated in iPP/aPS/uPP-*g*-PS blends is characterized by crystalline lamellar thickness (L_c) and interlamellar amorphous layer thickness (L_a) higher than that shown by plain iPP; the higher the copolymer content, the higher the L_c and L_a. It should be remarked that considerably larger increases have been found in L_a values. Such SAXS results have been accounted for by assuming that a cocrystallization phenomenon between propylenic sequences of the uPP-*g*-PS copolymer and iPP occurs and that during such a process PS chains grafted into copolymer sequences remain entrapped in iPP interlamellar amorphous layers, where they form their own separate domains. J Appl Polym Sci **65:** 1539–1553, 1997

Key words: polypropylene; propylene-*g*-styrene; copolymer; blends; morphology; structure

INTRODUCTION

A novel graft copolymer of propylene with styrene (uPP-*g*-PS), obtained by grafting via metallation atactic polystyrene (aPS) along the backbone chain of an unsaturated propylene-butadiene copolymer containing 3% (wt/wt) of butadiene (uPP), has been added to binary blends constituted by commercial samples of isotactic polypropylene (iPP) and aPS. Both uPP and uPP-*g*-PS copolymers have been synthesized following pro-

Correspondence to: L. D'Orazio.
 CCC 0021-8995/97/081539-15

cesses patented by Cecchin and colleagues from Himont.[1,2] From such patents it has been shown that by using a proper catalyst system the configuration of the butadiene units can be controlled, allowing the achievement of copolymers of propylene with butadiene having the butadiene linked mainly in configuration 1,2,[1] and that such copolymers can be crosslinked or modified by reactions typical of the unsaturated polymers or the allylic hydrogens, such as: epoxidation, sulphonation, condensation with maleic anhydride, radical grafting of vinyl monomers, acrylic monomers, silanes, covulcanization with other unsaturated polymers, etc.[2] In previous work the results of molecular, structural, morphological, and thermal characterization of the uPP and uPP-*g*-PS copolymers have been already reported[3]; the same article also examined the influence of concentration and distribution of noncrystallizable comonomer units on the kinetic, morphological, and thermodynamic parameters related to crystallization process of the propylenic sequences from melt. As far as the uPP-*g*-PS copolymer used in this study is concerned, it was found that the PS phase is present in short blocks with frequent points of insertion, the PS being atactic. Wide angle X-ray scattering (WAXS) and differential scanning calorimetry (DSC) experiments showed that in uPP-*g*-PS copolymers there are propylenic sequences able to crystallize in the α form of iPP. The value of the equilibrium melting temperature (T_m) calculated according to the kinetic theory of polymer crystallization was found to be in good agreement with the T_m value obtained by plotting the apparent melting temperature versus the inverse of lamellar thickness by small angle X-ray scattering (SAXS). Such a T_m value is about 30 K lower than that reported in literature for iPP, indicating the presence of defects along the uPP-*g*-PS crystallizable sequences. As a matter of fact, a free energy of folding value much lower than that reported in literature for iPP confirmed a very irregular and perturbed surface of such crystals.[3]

In the present paper we report on results of investigations regarding samples of binary iPP/aPS and ternary iPP/aPS/uPP-*g*-PS blends. The goal of this study is twofold. On the one hand it is to assess whether the uPP-*g*-PS copolymer can be used for compatibilizing polypropylene with PS, or polypropylene with polyphenylene oxide and its blends with PS acting as interfacial agent. On the other hand is the goal to investigate, within the framework of our researches on iPP-based blends containing a second noncrystallizable component,[4–9] the morphological and structural variations induced by the addition of the uPP-*g*-PS copolymer in the crystalline texture of the iPP/aPS blends.

It is to be pointed out that the achievement of iPP-based blends compatibilized by means of modified uPP copolymers would open new opportunities to obtain high-value specialty iPP-based materials for application fields where reactivity or polarity are required; polypropylene, in fact, owing to its saturated hydrocarbon structure, cannot be used in such fields. Generally in immiscible blends, such as iPP/aPS blends, two effects are to be expected for the presence of compatibilizer at the interface: the adhesion between the phases increases and the interfacial tension between them decreases; the smaller phase size plus the increased phase adhesion resulting in improved physical properties.[10–13] Dynamic mechanical thermal analysis (DMTA), DSC, optical microscopy (OM), scanning electron microscopy (SEM), WAXS, and SAXS have therefore been used to investigate morphology and structure of phases and interphases developed in iPP/aPS/uPP-*g*-PS blends by addition of 2%, 5%, and 10% (wt/wt) of uPP-*g*-PS copolymer in solution-cast samples.

EXPERIMENTAL

Materials

The starting polymers used in this study were an iPP (HS005) made by Himont, an aPS made by Rapra, and a uPP-*g*-PS copolymer synthesized in the Himont scientific laboratories according to methods patented by Cecchin and associates from Himont.[1,2] The molecular characteristics of such materials are reported in Table I.

Blending and Sample Preparation

All the investigated samples were obtained by means of the solvent-casting method. The blend components were dissolved in a common solvent, *o*-dichlorobenzene, at a total polymer concentration of 3% by weight and at the temperature of 135°C. Thin films were then obtained by *o*-dichlorobenzene casting carried out under vacuum at the temperature of 135°C for 3 h. iPP/aPS (80/20 wt/wt) binary blends and iPP/aPS/uPP-*g*-PS ternary blends containing 2%, 5%, and 10% (wt/wt) of graft copolymer were prepared.

Table I Molecular Characteristics of the Starting Polymers Together with T_g, T'_m, and X_c

Sample	$\bar{M}_n$ (g/mol)	$\bar{M}_w$ (g/mol)	$\bar{M}_w/\bar{M}_n$	η (dl/g)	% PS (wt/wt)	T_g[a] (°C)	T'_m[b] (°C)	X_c[c]
iPP	78,700	509,000	6.5	2.0	—	7	164	0.47
aPS	74,300	291,000	3.9	—	100	115	—	—
uPP-*g*-PS	—	—	—	1.4	35	11 118	142	0.20

[a] Glass transition temperature.
[b] Apparent melting temperature.
[c] Crystallinity index.

Techniques

Differential Scanning Calorimetry

The thermal behavior of the thin films of plain starting components and blends as obtained by casting was analyzed by means of a Differential Scanning Calorimeter with a Mettler TA 3000 instrument equipped with a control and programming unit (microprocessor Tc 10). The apparent melting temperatures (T'_m) and the crystallinity index (X_c) were determined following this procedure: the samples (about 9 mg) were heated from room temperature to 215°C at a rate of 10°C/min and the heat evolved during the scanning process was recorded as a function of temperature. The observed melting temperatures (T'_m) and the apparent enthalpies of melting (ΔH^*) were obtained from the maxima and the area of the melting peaks, respectively. The X_c of iPP and of blends were calculated by applying the following relations:

$$X_c(\text{iPP}) = \Delta H^*(\text{iPP})/\Delta H^0(\text{iPP}) \quad (1)$$

$$X_c(\text{blend}) = \Delta H^*(\text{blend})/\Delta H^0(\text{iPP}) \quad (2)$$

where ΔH^*(iPP) is the apparent enthalpy of fusion per gram of iPP in the blend; ΔH^0(iPP) is the heat of fusion per gram of 100% crystalline iPP, from 14 ΔH^0(iPP) = 209 J/g; and ΔH^*(blend) is the apparent enthalpy of fusion per gram of blend. The crystalline weight fractions referred to the iPP phase in blends [X_c(iPP)] were calculated from the following relation:

$$X_c(\text{iPP}) = X_c(\text{blend})/W(\text{iPP}) \quad (3)$$

where W(iPP) is the weight fraction of iPP in the blends.

The effect of nucleating ability of aPS and uPP-*g*-PS copolymer on the crystallization process of iPP was investigated following this procedure: the samples were heated to 215°C at a rate of 10°C/min and kept at this temperature for 10 min in order to destroy any traces of crystallinity, then cooled at a rate of 10°C/min.

Dynamic Mechanical Thermal Analysis

The tangent δ and storage modulus of all investigated samples were measured by means of a Dynamic Mechanical Thermal Analyzer (Rheometric Scientific MK III). Test data were collected in the tensile mode from −40°C to 140°C using a scanning rate of 1.5°C/min and a frequency of 1 Hz.

Optical Microscopy

The thin films of plain starting components and blends as obtained from solution casting were observed by means of OM. A Leitz optical polarizing microscope fitted with a Mettler hot stage was used; optical micrographs were taken with crossed and parallel polarizers.

Scanning Electron Microscopy

Cryogenically fractured surfaces of thin films of binary and ternary blends were observed by means of a Philips XL 20 Scanning Electron Microscope after coating with gold-palladium.

Wide Angle X-ray Scattering

WAXS studies were carried out by means of a PW 1060/71 Philips diffractometer (CuKα Ni-filtered radiation) equipped with a sample carrier for sample spinning; high voltage was 40 KV and tube current was 30 mA. A standard sample was employed to determine the instrumental broadening.

Small Angle X-ray Scattering

SAXS studies were carried out by means of a compact Kratky camera equipped with a Braun one-

Table II Thermal Behavior of Polymers

Sample	T_g[a] (°C)	T_m[b] (°C)	X_c (blend)[c]	X_c (iPP)[d]
iPP/aPS	3 117	164	0.38	0.47
iPP/aPS/uPP-*g*-PS graft 2% (wt/wt)	4 116	164	0.39	0.49
iPP/aPS/uPP-*g*-PS graft 5% (wt/wt)	4 116	165	0.38	0.48
iPP/aPS/uPP-*g*-PS graft 10% (wt/wt)	5 116	164	0.37	0.47

[a] Glass transition temperature.
[b] Apparent melting temperature.
[c] Crystallinity index of the binary iPP/aPS and ternary iPP/aPS/uPP-*g*-PS blends.
[d] Crystallinity index of iPP phase.

dimensional positional sensitive detector. Ni-filtered CuKα radiation generated from a Philips X-ray generator (PW 1730/10), operating at 40 KV and 30 mA, was used. The raw scattering data were corrected for parasitic scattering, absorption, and slit smearing by using Vonk's method.[15] The desmeared intensities were then Lorentz factor-corrected by multiplying by s^2 ($s = 2 \sin \theta/\lambda$).[16]

RESULTS AND DISCUSSION

Thermal Behavior

The glass transition temperatures (T_g) of the plain starting polymers detected by DMTA measurements are reported in Table I. Note that the uPP-*g*-PS copolymer exhibits two distinct T_g to be attributed to iPP and aPS phases, respectively; each resulting T_g value being higher than that shown by the plain iPP and aPS, respectively. The variation of tangent δ with temperature obtained for the binary iPP/aPS and ternary iPP/aPS/uPP-*g*-PS blends shows that the iPP/aPS blend possesses individual T_g of the single components, as expected for immiscible polymer blend systems; moreover, regardless of blend composition, no significant shift in such T_g values after the addition of the uPP-*g*-PS copolymer is observed (see Table II). Such a finding seems to indicate immiscibility of the uPP-*g*-PS phase with both iPP and PS phase in the amorphous condensed state.

The DSC thermograms of the binary iPP/aPS and ternary iPP/aPS/uPP-*g*-PS blends show a single endothermic peak when heated from room temperature to 200°C. To be noted is that such a peak widens with uPP-*g*-PS addition and that the extent of such an effect is composition-dependent; the observed broadening, in fact, increases on increasing the uPP-*g*-PS content (see Fig. 1). The temperatures corresponding to the maxima of such peaks (T'_m) are reported in Table II together with the crystallinity index of the blends [X_c(blend)] and of the iPP phase [X_c(iPP)]. From such data it emerges that the T'_m, X_c(blend), and X_c(iPP) values are almost independent of blend composition, being quite comparable to that shown by the plain iPP. Notwithstanding this, the finding that crystals grown in presence of uPP-*g*-PS phase show perfection decreasing and/or size distribution widening with higher copolymer content in the blend (see Fig. 1), suggesting that the uPP-*g*-PS copolymer interferes with the iPP crystallization process. The DSC thermogram of the plain uPP-*g*-PS copolymer shows that a double melting peak is exhibited by such a copolymer, the first being broader and lower than the second (see Fig. 2). The temperature positions of such peaks are reported in Table I and are considerably lower than that shown by the iPP phase. Taking into account that, regardless of copolymer content in the blend, no separate melting of the uPP-*g*-PS propylenic sequences is detected, it could be hypothesized that such sequences are able to cocrystallize with the iPP allowing the formation of crystalline phases with different perfections and/or thicknesses.

The curve of non-isothermal crystallization from melt of the plain iPP is compared with those shown by the iPP phase non-isothermally crystal-

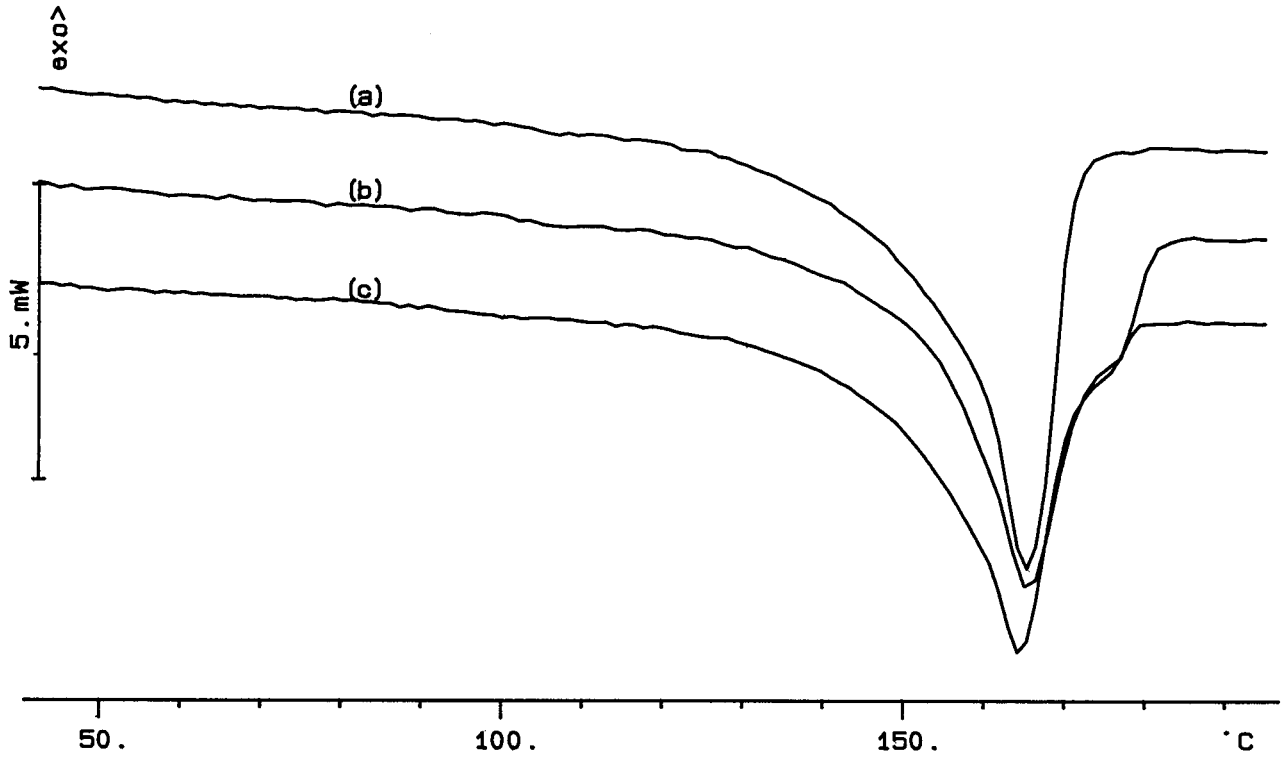

Figure 1 DSC thermograms of binary iPP/aPS (a) and ternary iPP/aPS/uPP-*g*-PS blends containing 2% (wt/wt) (b) and 10% (wt/wt) (c) of uPP-*g*-PS copolymer.

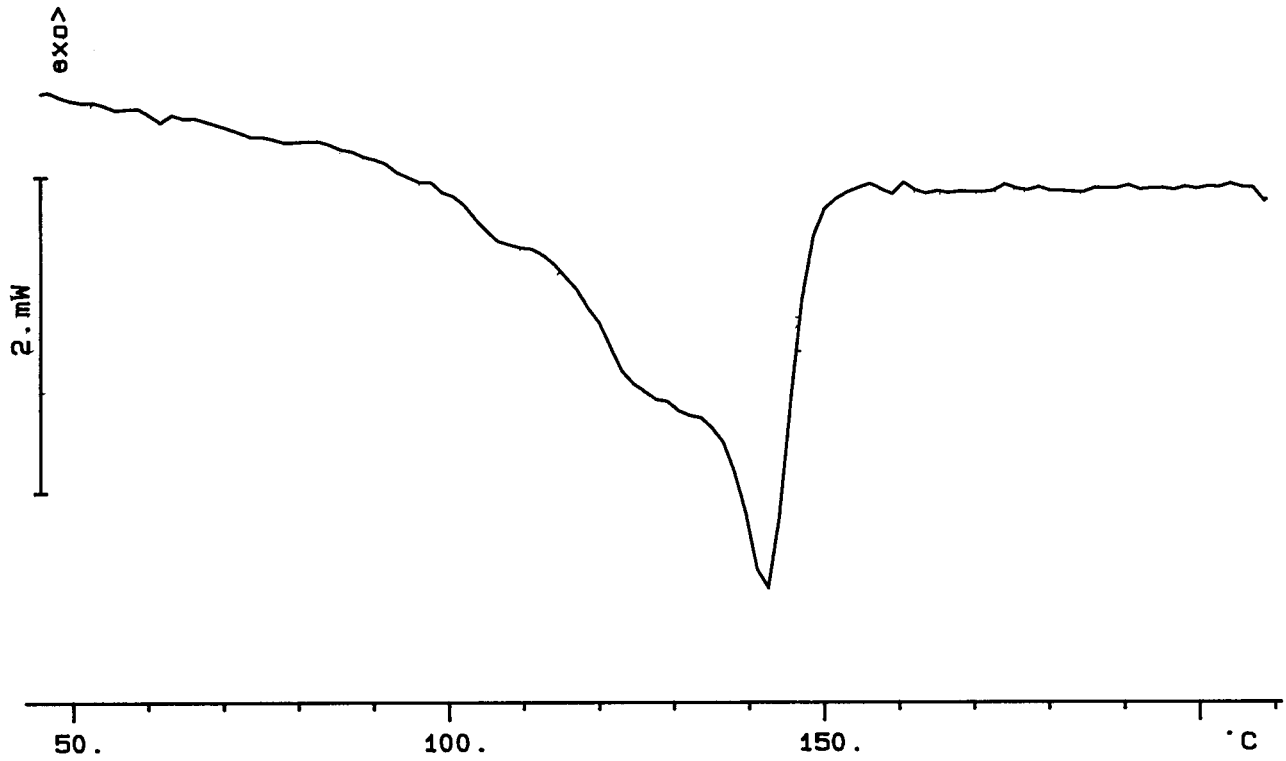

Figure 2 DSC thermogram of plain uPP-*g*-PS copolymer.

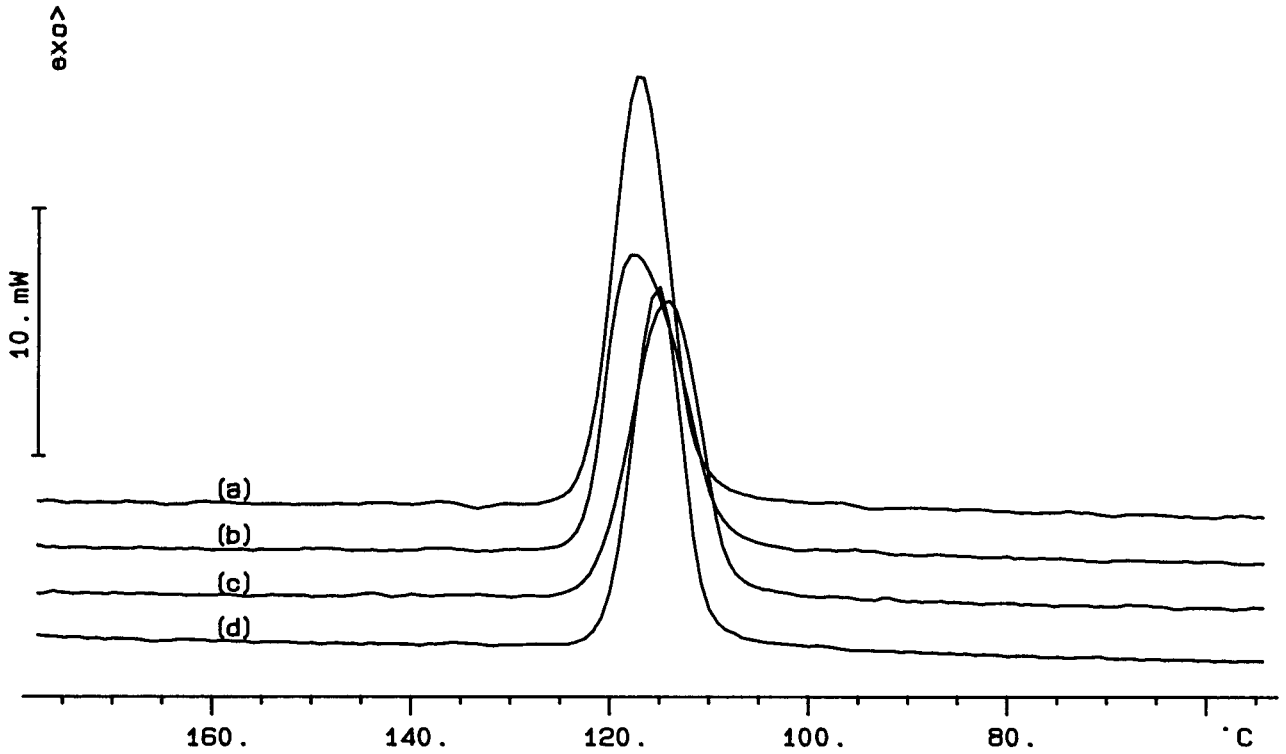

Figure 3 Nonisothermal crystallization curves for plain iPP (a) and for iPP phase crystallized from its binary iPP/aPS blends (b) and ternary iPP/aPS/uPP-*g*-PS blends containing 2% (wt/wt) (c) and 10% (wt/wt) (d) of uPP-*g*-PS copolymer.

lized from melts of the binary iPP/aPS and ternary iPP/aPS/uPP-*g*-PS blends in Figure 3. As shown when the iPP crystallizes in the presence of aPS, the range of crystallization temperature remains comparable to that shown by the plain iPP, indicating that the aPS used in this work has no nucleating ability on the crystallization process of the iPP. A slight shift of the crystallization peak to lower temperatures is, on the other hand, exhibited by the iPP crystallizing from its ternary blends; moreover, the observed shift increases with increasing content of the uPP-*g*-PS phase in the blend (see Fig. 3 and Table III). Such findings indicate that not even the uPP-*g*-PS copolymer has nucleating ability on the crystallization process of the iPP and that, on the contrary,

Table III Crystallization Behavior of Polymers

Sample	Nonisothermal Crystallization Range (°C)	T'_m [a] (°C)	X_c (blend)[b]	X_c (iPP)[c]
iPP	128–101	162	0.43	0.43
iPP/aPS	128–99	163	0.36	0.43
iPP/aPS/uPP-*g*-PS graft 2% (wt/wt)	127–99	162	0.33	0.41
iPP/aPS/uPP-*g*-PS graft 5% (wt/wt)	126–99	163	0.33	0.42
iPP/aPS/uPP-*g*-PS graft 10% (wt/wt)	126–97	161	0.33	0.42
uPP-*g*-PS	113–85	142	0.20	0.32

[a] Apparent melting temperature.
[b] Blend crystallinity index.
[c] Crystallinity index of iPP phase.

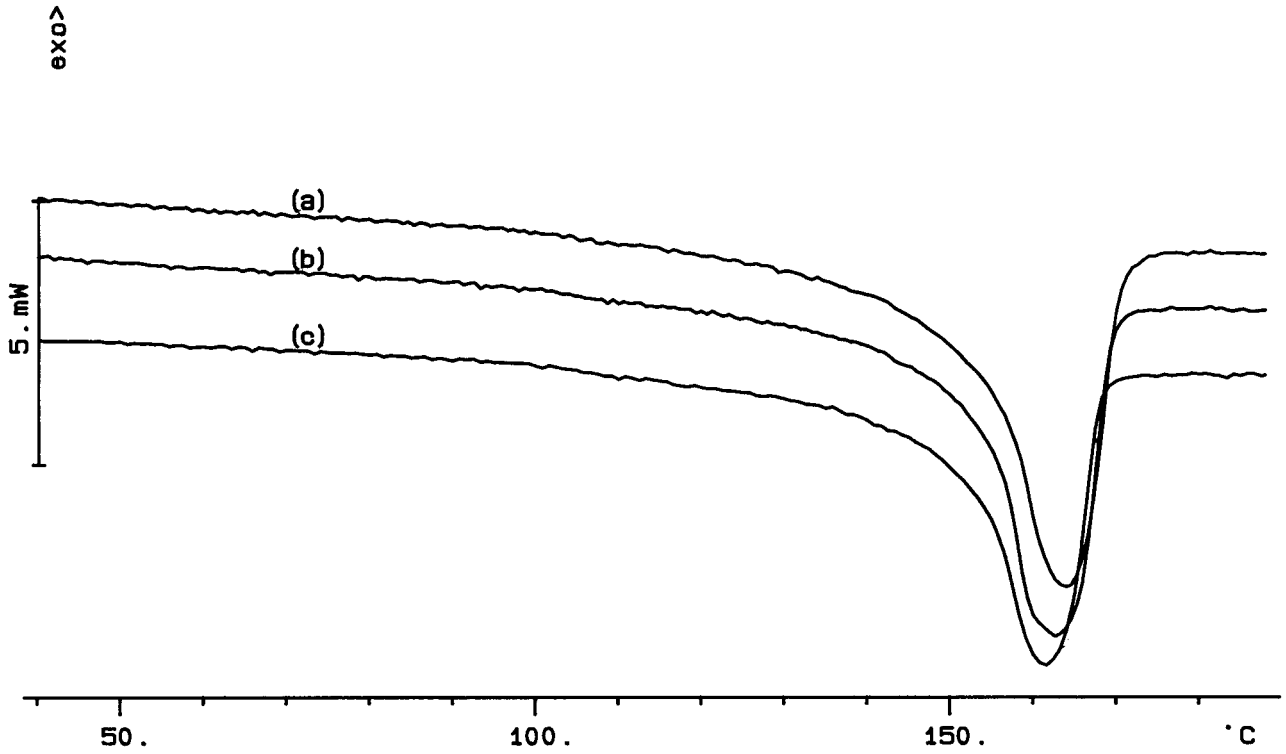

Figure 4 DSC thermograms of nonisothermally crystallized samples of binary iPP/aPS (a) and ternary iPP/aPS/uPP-*g*-PS blends containing 2% (wt/wt) (b) and 10% (wt/wt) (c) of uPP-*g*-PS copolymer.

a migration of heterogeneous nuclei, which increases with increasing the copolymer content in the blend, occurs from the iPP phase toward the uPP-*g*-PS phase. To be pointed out also is that the uPP-*g*-PS copolymer shows a range of nonisothermal crystallization fully included in that shown by the plain iPP, indicating that its crystallization process from the melt is strongly correlated with that of the plain iPP.

The DSC thermograms of nonisothermally crystallized samples of binary and ternary blends are shown in Figure 4; a single endothermic peak, when heated from room temperature to 200°C, is exhibited by all the investigated samples in agreement with the thermal behavior shown by the samples obtained from solution-casting. The temperature position of the maxima of the observed peaks (T'_m), X_c(blend), and X_c(iPP) values are reported in Table III; the trend of such data agrees with that found for the cast samples even though, owing to the crystallization conditions imposed, such values are lower than that shown by the iPP phase in the solution-cast samples (compare Tables II and III). From the evidence obtained by the DSC experiments, the iPP and uPP-*g*-PS copolymer could, at least in principle, either cocrystallize or separately crystallize. Moreover, occurrence of specific interactions in the amorphous melted state between the iPP and uPP-*g*-PS copolymer cannot be excluded; work is in progress to estimate the state of mixing of such components by studying phase behavior of binary iPP/uPP-*g*-PS blends.

Phase Structure

Microscopy Studies

Figure 5 shows optical micrographs, taken at crossed and parallel polars, of thin films of the binary (80/20 wt/wt) iPP/aPS blend; for sake of comparison, the optical micrographs of thin films of the plain iPP and uPP-*g*-PS copolymer are also shown. As shown, the iPP/aPS blend exhibits a well-defined spherulitic superstructure with the aPS phase segregated in spherical domains uniformly occluded in the iPP intra- and interspherulitic regions. Furthermore, neither does the amorphous material appear to be rejected at the spherulitic boundary regions nor are amorphous interspherulitic contact regions developed. On the other hand, the plain iPP shows large amorphous regions in agreement

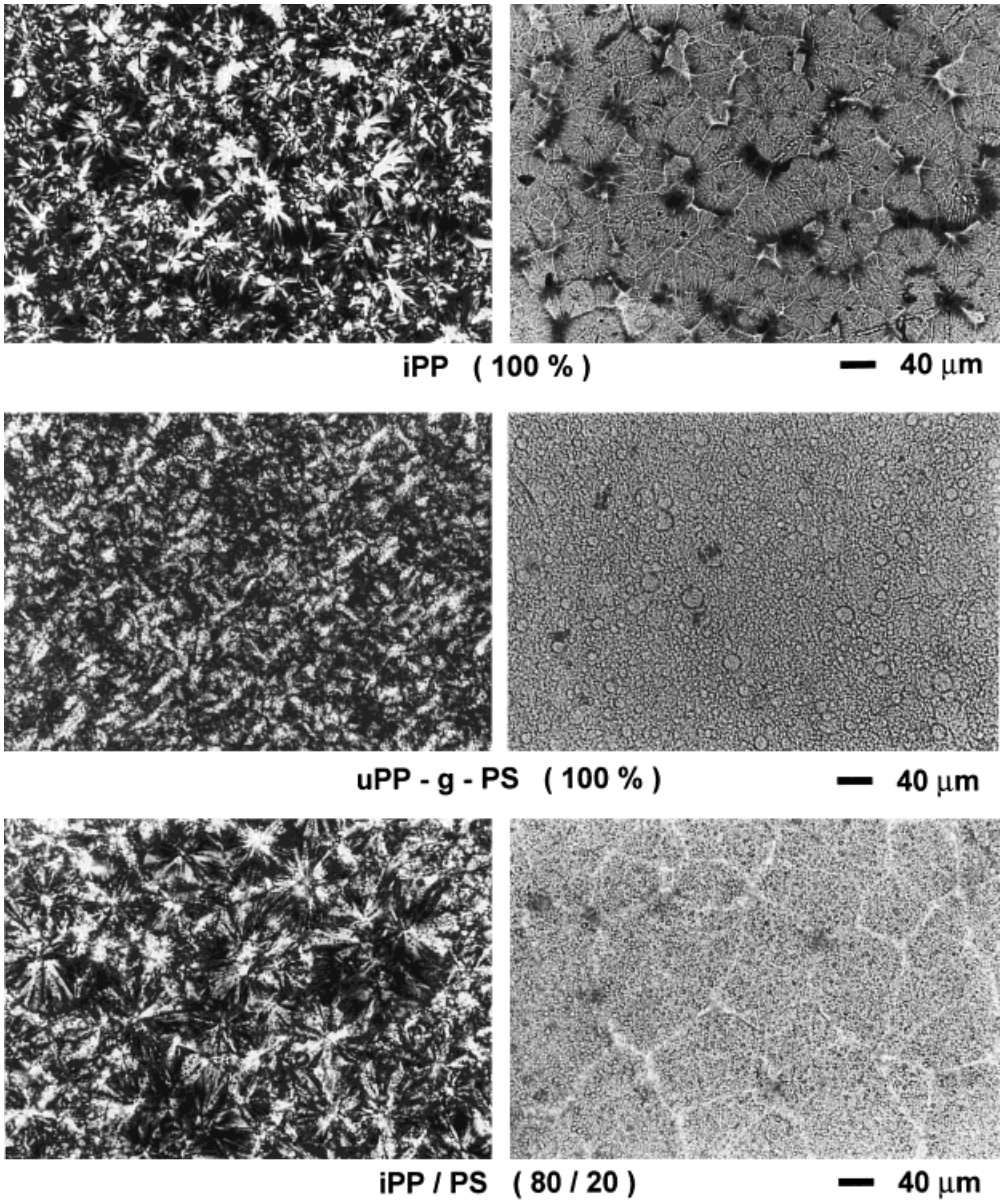

Figure 5 Optical micrographs taken at crossed and parallel polarizers of thin films of binary iPP/aPS blends and plain iPP and uPP-*g*-PS copolymer.

with results obtained by studying the influence of the crystallization conditions on the structure of phases and interphase developed after complete crystallization of the iPP under controlled crystallization conditions.[5] As far as crystalline texture shown by the plain uPP-*g*-PS copolymer is concerned, note that the spherulites appear damaged in their neatness and regularity; this finding has been related to the distribution of the PS chains that, owing to their high number and shortness, were found to interfere strongly with the crystallization process of the copolymer propylenic sequences.[3] From the SEM investigations performed on transversally cryogenically fractured surfaces of iPP/aPS films, the aPS particles show a relatively narrow size distribution, with diameters ranging between 1.5 and 4.3 μm; moreover, the smooth surfaces of debonded particles and the clean holes where the particles separated from the iPP matrix during the fracture show poor adhesion between the phases.

With added uPP-*g*-PS copolymer, the phase morphology developed in the blends is dramatically modified. As far as the spherulitic texture is concerned, the iPP phase crystallized from its ternary blends forms spherulites whose size, neat-

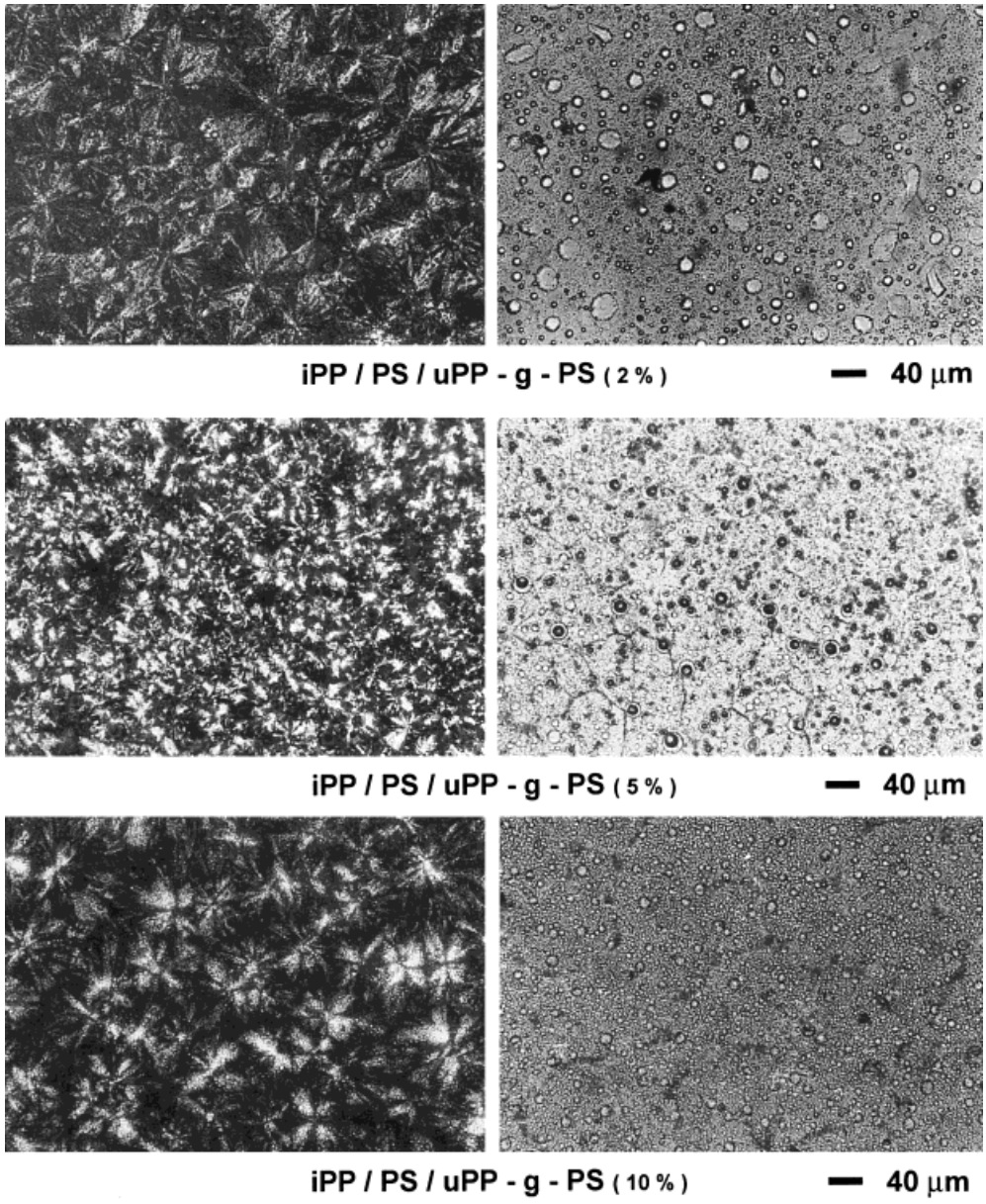

Figure 6 Optical micrographs taken at crossed and parallel polarizers of thin films of iPP/aPS/uPP-*g*-PS ternary blends containing 2%, 5%, and 10% (wt/wt) of uPP-*g*-PS copolymer, progressively.

ness, and regularity are slightly composition-dependent. As a matter of fact, for low uPP-*g*-PS content (2% wt/wt), the iPP spherulitic superstructure appears comparable to that shown by the iPP phase crystallized from its iPP/aPS binary blends, and with increased uPP-*g*-PS content a perceptible, but not great, reduction in size, neatness, and regularity of the formed spherulites is observed (see Fig. 6). On the other hand, deep changes in the aPS mode and state of dispersion by the uPP-*g*-PS addition are caused. In the blends containing the 2% (wt/wt) of the graft copolymer the aPS domains show a very broad distribution of particle size that seems to tend toward bimodality. The visual impressions of the morphologies shown in Figure 6 are confirmed by quantitative image analysis of several SEM photomicrographs of this blend. There is a population of aPS particles with diameters in the range of 0.1–0.5 μm and another population of particles in the size range of 1.5–7.0 μm (see Fig. 7); such a range being noticeably larger than that shown by the PS phase in the iPP/aPS binary blends. The dispersion degree of the minor component

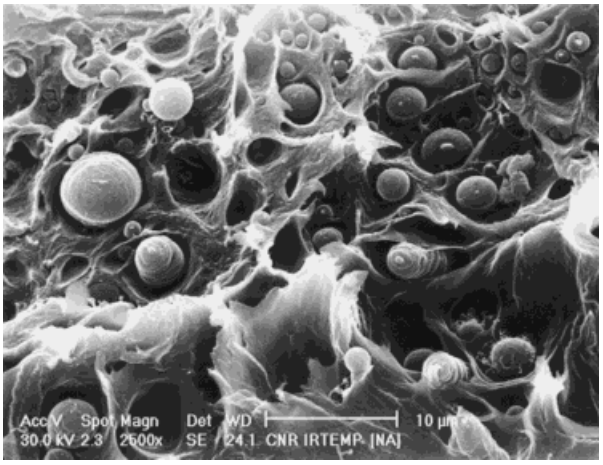

Figure 7 SEM micrographs of cryogenical fracture surfaces of iPP/aPS/uPP-*g*-PS ternary blends containing 2% (wt/wt) of uPP-*g*-PS copolymer (2,500×).

Figure 9 SEM micrographs of cryogenical fracture surfaces of iPP/aPS/uPP-*g*-PS ternary blends containing 5% (wt/wt) of uPP-*g*-PS copolymer (5,000×).

achieved by adding the 2% (wt/wt) of the uPP-*g*-PS copolymer suggests that the extent of compatibilization is not essentially the same for each PS-based particle formed. The above results could be accounted for in terms of uneven dispersion of the graft copolymer and/or in terms of a different state of mixing of uPP-*g*-PS copolymer with iPP and aPS. SEM analysis reveals, moreover, that the aPS particles are coated by a smooth interfacial layer; if interfacial failure occurs, such a layer tends to cluster around the aPS particles, suggesting that the uPP-*g*-PS copolymer forms a deformable shell around them (see Fig. 8). Such a morphological result can be modeled according to a core–shell interfacial model consisting of three phases: matrix, dispersed particles, and copolymer shell on particles with quite comparable adhesion to both particle core and matrix.[17]

With increased uPP-*g*-PS content to 5% (wt/wt), the particle size distribution becomes comparatively narrower and a single average can be calculated, indicating that a more homogeneous system has been achieved. The particle diameters are in the range of 1.0–2.5 μm; note that such a dispersion degree is finer than that found for iPP/aPS blends. The transversely cryogenically fractured surfaces of thin films of this ternary blend provide evidence of interfacial adhesion with fibrils connecting the phases (see Fig. 9). It is very interesting to note that, instead of a smooth coating on the aPS particles, a typical aPS particle retains a rough texture where the interface has

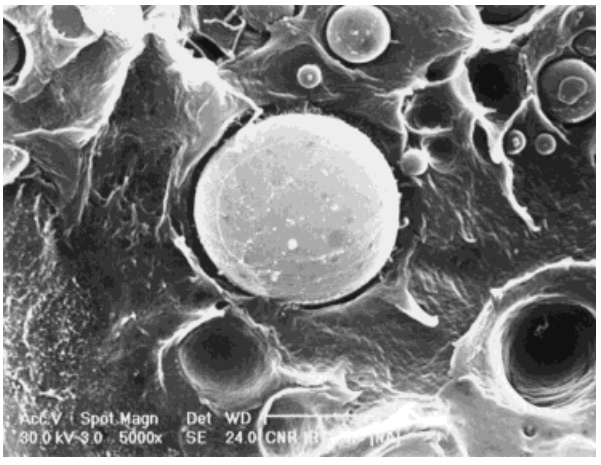

Figure 8 SEM micrographs of cryogenical fracture surfaces of iPP/aPS/uPP-*g*-PS ternary blends containing 2% (wt/wt) of uPP-*g*-PS copolymer (5,000×).

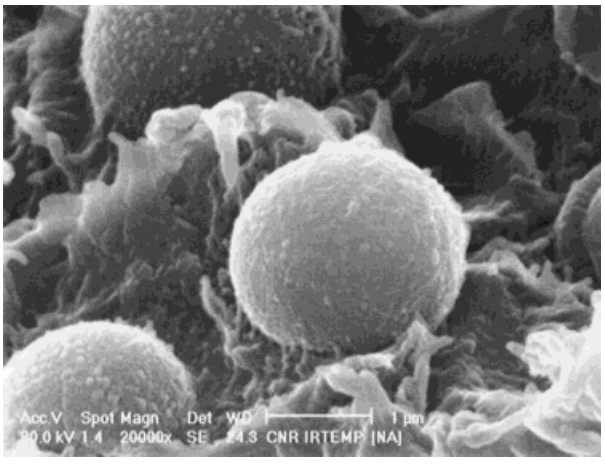

Figure 10 SEM micrographs of cryogenical fracture surfaces of iPP/aPS/uPP-*g*-PS ternary blends containing 5% (wt/wt) of uPP-*g*-PS copolymer (20,000×).

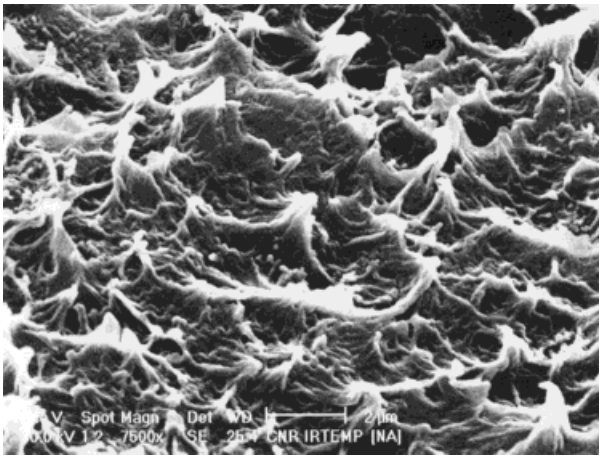

Figure 11 SEM micrographs of cryogenical fracture surfaces of iPP/aPS/uPP-*g*-PS ternary blends containing 10% (wt/wt) of uPP-*g*-PS copolymer (7,500×).

fractured, suggesting that in this case that the uPP-*g*-PS copolymer interpenetrated the aPS phase (see Fig. 10).

SEM micrographs of transversely fractured surfaces of the iPP/aPS/uPP-*g*-PS blends containing 10% (wt/wt) of the copolymer are shown in Figure 11. As shown, such a material exhibits such a homogeneous texture that dispersed phase cannot be clearly detected. Investigations performed at very high magnification (30,000×) reveal the presence of particles whose maximum diameter is ≤ 0.2 μm; no holes where such particles separated can be observed. Moreover, it should be pointed out that the fracture occurs in a ductile manner with evidence of plastic deformation. Such morphological results indicate that the uPP-*g*-PS copolymer is capable of selectively penetrating its homopolymer phases to provide good interconnection in between. The type of interface developed in such iPP/aPS/uPP-*g*-PS blends could be then accounted for by an interpenetration model; according to such a model the average interfacial area stabilized per copolymer molecule should be a constant.[18,19]

Wide Angle X-ray Scattering Studies

Typical WAXS diffractograms of thin films of binary iPP/aPS and ternary iPP/aPS/uPP-*g*-PS blends are shown in Figures 12 and 13. As shown, all the samples give diffraction peaks whose angles are characteristic for the crystal structure of the α form of polypropylene and, in addition, show a broad, diffraction, noncrystalline halo. Such noncrystalline halo results are centered at $2\theta = 18°$ for the binary iPP/aPS blend; for the plain iPP and aPS such halos are centered at 2θ values of 16.6° and 19.5°, respectively. By adding 2% (wt/wt) of uPP-*g*-PS copolymer the noncrystalline halo of the resulting ternary blend shifts toward lower 2θ value (17.1°) closely approaching the 2θ value shown by the amorphous phase of the plain uPP-*g*-PS copolymer (17.2°). With increasing uPP-*g*-PS content, the halo shifts further toward higher angles: 17.4° and 18.2° for the blends containing, respectively, 5% (wt/wt) and 10% (wt/wt) of graft copolymer.

The apparent crystal size (D) of iPP in the perpendicular direction to the (110), (040), and (130) crystallographic planes was calculated by the Sherrer equation[16]:

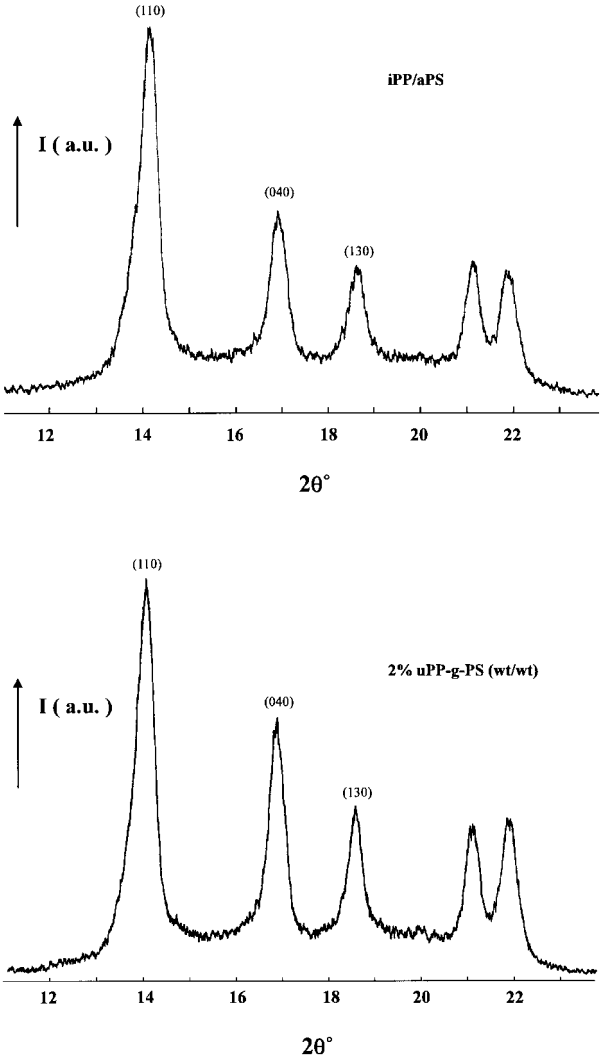

Figure 12 WAXS diffractograms of binary iPP/aPS blends and iPP/aPS/uPP-*g*-PS ternary blends containing 2% (wt/wt) of uPP-*g*-PS copolymer.

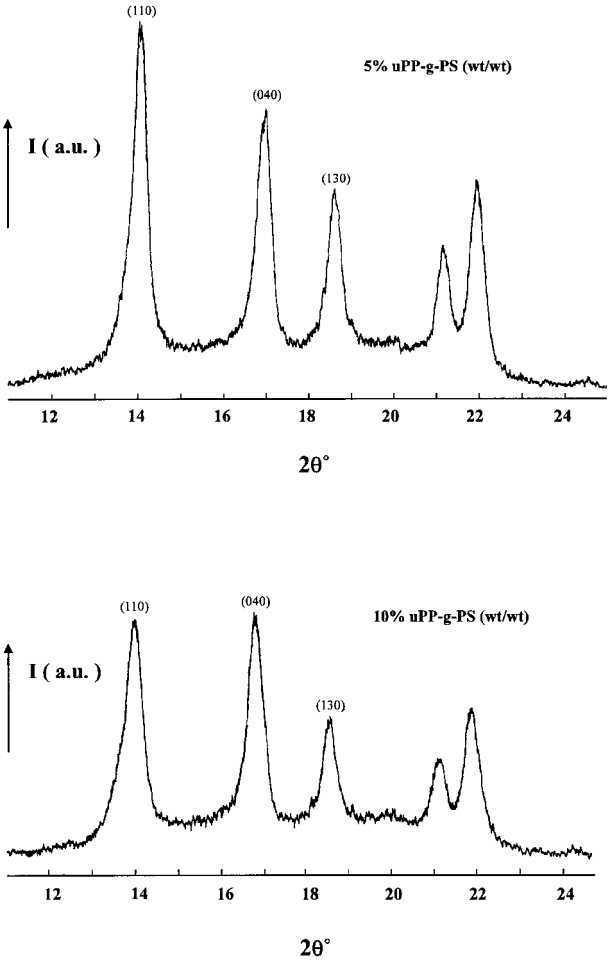

Figure 13 WAXS diffractograms of iPP/aPS/uPP-*g*-PS ternary blends containing 5% and 10% (wt/wt) of uPP-*g*-PS copolymer.

$$D_{\mathrm{hkl}} = \frac{K\lambda}{\beta_0 \cos(\theta_{\mathrm{hkl}})}$$

where β_0 is the half-width in radians of the reflection corrected for instrumental broadening, and λ is the wavelength of the radiation used (1.5418 Å). The shape factor K is set equal to unity, so the size data have to be considered as relative data. The absence in the WAXS diffractograms of (220) reflection did not allow correction for lattice distortion of D (110). The crystal sizes of both binary and ternary blends are higher than that of the plain iPP, a comparatively larger size being shown by iPP phase crystallized from the ternary blends containing 5% (wt/wt) of uPP-*g*-PS copolymer (see Table IV). Such findings indicate a higher growth of the iPP crystals in the blends with no systematic dependence upon the composition.

Small Angle X-ray Scattering Studies

Typical Lorentz-corrected desmeared patterns for samples of binary iPP/aPS and ternary iPP/aPS/uPP-*g*-PS blends are shown in Figure 14. These SAXS profiles exhibit well-defined maxima; by applying Bragg's law the long period (L) of the iPP phase has been calculated from the peak position. It is interesting to observe that the peak positions for the ternary blends shift to comparatively lower angles and that such an effect is composition-dependent. Assuming a two-phase model for the iPP spherulite fibrillae, consisting of alternating parallel crystalline lamellae and amorphous layers, the crystalline lamellar thickness (L_c) has been calculated using the following relation for the L values:

$$L_c = \frac{X_{c\,(\mathrm{iPP})} L}{(\rho_c/\rho_a)(1 - X_{c\,(\mathrm{iPP})}) + X_{c\,(\mathrm{iPP})}}$$

where $X_{c\,(\mathrm{iPP})}$ is the DSC crystallinity index of the iPP phase; and ρ_c and ρ_a are the densities of the crystalline and amorphous iPP phases, respectively.

The thickness of the amorphous interlamellar layer (L_a) has been calculated by

$$L_a = L - L_c$$

The L, L_c, and L_a of the plain iPP, and of iPP crystallized from its binary and ternary blends, are reported in Table V. As shown for the plain iPP and iPP crystallized from the iPP/aPS blends, the L, L_c, and L_a values are within experimental error (50 nm), confirming that the iPP phase structure remains uneffected by the presence of PS phase. On the other hand, for the ternary blends, L values increase markedly with increasing uPP-*g*-PS content. According to the model used, the surprising increase of L with uPP-*g*-PS composition is due to the increase in both the average crystalline thickness and interlamellar amorphous phase (see Table V and the trends of plots of Fig. 15). Thus when iPP crystallizes in presence of the uPP-*g*-PS copolymer, the phase structure developed in the blends can be characterized by L_c and L_a higher than that shown by plain iPP. Note that the increase observed in L_a value is higher than that found for L_c values (see Fig. 15 and Table V). These results can be accounted for by the development in the iPP/aPS/uPP-*g*-PS blends of a lamellar structure of the iPP phase such as that schematically modelled in Figure 16 as a function of the uPP-*g*-PS content (wt/

Table IV Apparent Crystal Size (D) of Plain iPP, Its Binary and Ternary Blends, and Plain uPP-*g*-PS Copolymer

Sample	$D_{(110)}$ (Å)	$D_{(040)}$ (Å)	$D_{(130)}$ (Å)
iPP	77	112	85
iPP/aPS	94	99	105
iPP/aPS/uPP-*g*-PS graft 2% (wt/wt)	105	112	105
iPP/aPS/uPP-*g*-PS graft 5% (wt/wt)	105	128	119
iPP/aPS/uPP-*g*-PS graft 10% (wt/wt)	85	112	112
uPP-*g*-PS	52	105	—

wt). According to the proposed model, a co-crystallization phenomenon occurs among propylenic sequences of the uPP-*g*-PS copolymer and iPP. During such a process, PS chains grafted into copolymer sequences, probably owing to their shortness, remain entrapped in the iPP interlamellar amorphous regions, where they form their own separated domains. Work is in progress to assess the validity of such a model, investigating the structure of phase and interphases developed in binary iPP/uPP-*g*-PS

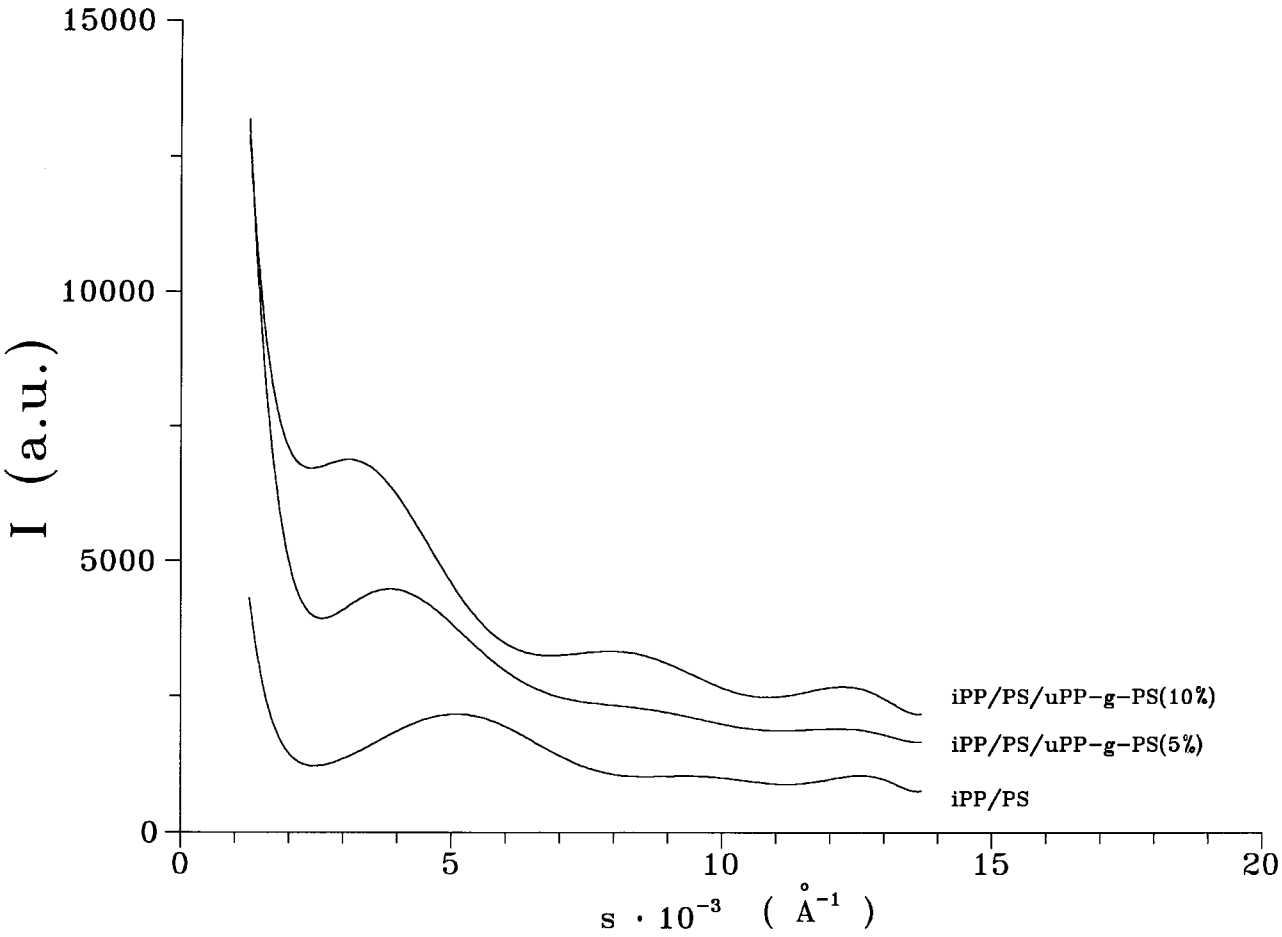

Figure 14 Typical SAXS Lorentz-corrected desmeared patterns of iPP/aPS binary and iPP/aPS/uPP-*g*-PS ternary blends.

Table V Long Period (L), Crystalline Lamella Thickness (L_c) and Interlamellar Amorphous Thickness (L_a) for Plain iPP, Its Binary and Ternary Blends, and Plain uPP-*g*-PS Copolymer

Sample	L (Å)	L_c (Å)	L_a (Å)
iPP	197	88	109
iPP/aPS	195	87	108
iPP/aPS/uPP-*g*-PS graft 2% (wt/wt)	220	103	117
iPP/aPS/uPP-*g*-PS graft 5% (wt/wt)	260	119	141
iPP/aPS/uPP-*g*-PS graft 10% (wt/wt)	321	143	178
uPP-*g*-PS	115	33	82

blends after complete iPP crystallization for controlled undercooling and annealing.

CONCLUSIONS

Blends of iPP and aPS exhibit coarse domain morphology that is characteristic of immiscible blends. The study performed on the capability of a novel graft copolymer of propylene with styrene (uPP-*g*-PS) to act as compatibilizer for iPP/aPS blends, with the focus on iPP/aPS (80/20) composition, led to the conclusions that the uPP-*g*-PS addition can provide iPP/aPS compatibilized materials and that the extent of the compatibilization achieved is composition-dependent. A 2% addition (wt/wt) of uPP-*g*-PS phase induces a very broad distribution of PS particles, tending toward bimodality, presumably attributable to uneven distribution of the graft and/or to different states of mixing of uPP-*g*-PS phase with iPP and aPS phases. The aPS particles appear coated by a smooth interfacial layer; if interfacial failure occurs, such a coating layer tends to cluster, suggesting that the uPP-*g*-PS copolymer forms a deformable shell around the aPS particles. The type of interface developed in such a blend has been modeled according to a core–shell model. In the blends containing the 5% (wt/wt) of uPP-*g*-PS copolymer, a finer dispersion degree is achieved; the aPS particle size distribution function being continous. Moreover there is evidence of interfacial adhesion and fibrils connecting the phases. A typical aPS particle on a cryogenically fractured surface retains a rough texture where the interface has fractured, suggesting that in this case the graft copolymer interpenetrated the aPS phase. With further increased uPP-*g*-PS content (10% wt/wt), the blends show a texture so homogeneous that neither domains of dispersed phase nor holes can be clearly detected. From such morphological results it has been deduced that an almost-complete penetration of the uPP-*g*-PS copolymer in the two homopolymer phases occurs. The type of interface generated by additions of copolymer larger than 2% (wt/wt) has been modeled according to an interfacial interpenetration model. As far as the crystalline texture of iPP phase crystallized from its iPP/aPS/uPP-*g*-PS blends is concerned, WAXS diffractograms of the thin films of all the ternary blends investigated exhibit diffraction peaks whose angles are charac-

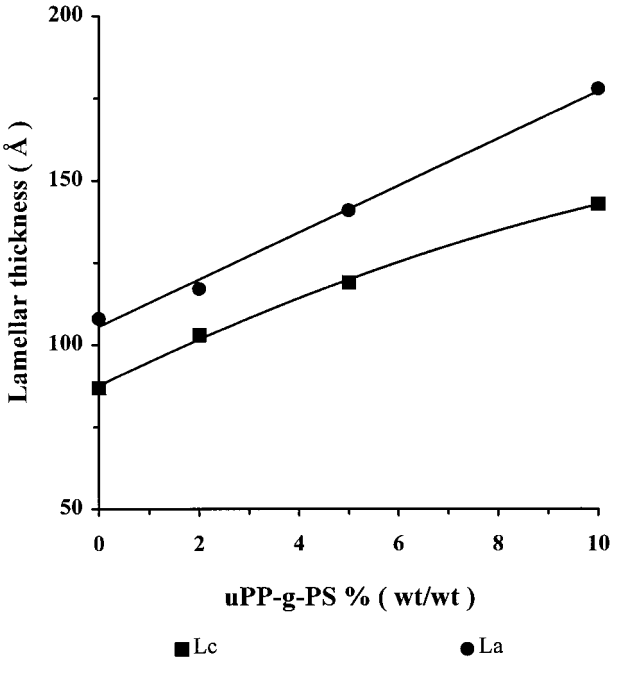

Figure 15 Plots of L_c and L_a of iPP phase as a function of uPP-*g*-PS copolymer content.

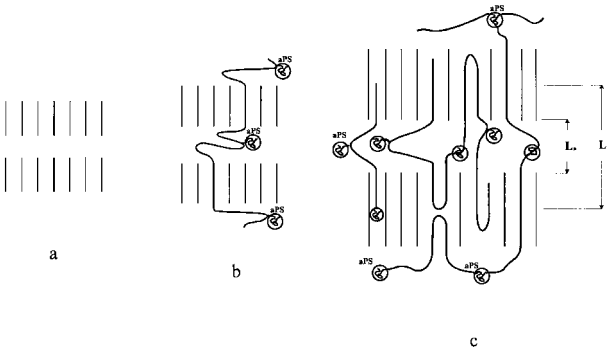

Figure 16 Schematic model of the iPP lamellar structure developed in iPP/aPS/uPP-*g*-PS blends as a function of uPP-*g*-PS content (wt/wt): a) 0%, b) 2%, c) 10%.

teristic for the crystal structure of the α form of polypropylene. Optical micrographs of the thin films of such blends, taken with crossed or parallel polarizers, show that the size, neatness, and regularity of the iPP spherulites decrease with slightly increased uPP-*g*-PS content. Assuming for the iPP spherulite fibrillae a two-phase model constituted by alternating parallel crystalline lamellae and amorphous layers, SAXS investigations reveal that the phase structure developed in iPP/aPS/uPP-*g*-PS blends is characterized by L_c and L_a higher than that shown by plain iPP and higher with higher copolymer content. To be underlined is that the extent of such an increase is larger for L_a values. Such SAXS results have been accounted for by modeling the lamellar structure of the iPP phase developed in the iPP/aPS/uPP-*g*-PS blends as follows: Propylenic sequences of the uPP-*g*-PS copolymer have been assumed to cocrystallize with iPP; during such a process, PS chains grafted into copolymer sequences, probably because of their shortness, remain entrapped in iPP interlamellar amorphous layers, where they form their own separate domains.

Evidence of a strong correlation between the crystallization process of the uPP-*g*-PS copolymer and the iPP crystallization process has also been shown by DSC experiments. The thermograms of both solution-cast and nonisothermally crystallized samples of iPP/aPS/uPP-*g*-PS blends exhibit, in fact, a single endothermic peak that widens with increasing copolymer content, showing that perfection and thickness of iPP crystal are noticeably affected by the copolymer presence. Work is in progress to extend the study of the iPP crystallization process to melts containing different amounts of uPP-*g*-PS copolymer and to the structure of phases and interphases developed in such binary blends after complete iPP crystallization for controlled undercooling and annealing.

REFERENCES

1. G. Cecchin, F. Guglielmi, and F. Zerega, U.S. Pat. 4,602,077 (1986).
2. G. Cecchin and A. DeNicola, U.S. Pat. 5,159,023 (1990).
3. L. D'Orazio, C. Mancarella, E. Martuscelli, and G. Sticotti, *J. Mat. Sci.,* **30,** 4960 (1995).
4. L. D'Orazio, C. Mancarella, and E. Martuscelli, *Polymer,* **32,** 1186 (1991).
5. L. D'Orazio, C. Mancarella, E. Martuscelli, and G. Sticotti, *J. Mat. Sci.,* **26,** 4033 (1991).
6. L. D'Orazio, C. Mancarella, E. Martuscelli, and G. Sticotti, *Polymer,* **34,** 3671 (1993).
7. L. D'Orazio, C. Mancarella, E. Martuscelli, and G. Sticotti, *J. Appl. Polym. Sci.,* **53,** 387 (1994).
8. L. D'Orazio, C. Mancarella, E. Martuscelli, and G. Sticotti, *Advanced Routes for Polymer Toughening,* Elsevier, Amsterdam, 1997 (in press), Chap. 5.
9. L. D'Orazio, C. Mancarella, E. Martuscelli, and G. Sticotti, *Polymer,* submitted.
10. D. R. Paul, in *Polymer Blends,* D. R. Paul and S. Newman, Eds., Academic Press, New York, 1978, p. 35.
11. G. Maglio and R. Palumbo, in *Polymer Blends,* M. Kryszewski, A. Galeski, and E. Martuscelli, Eds., Plenum Press, New York, 1982.
12. H. R. Brown, *Macromolecules,* **22,** 2859 (1989).
13. H. R. Brown, *Macromolecules,* **26,** 1166 (1993).
14. S. Brandrup and E. M. Immergut, *Polymer Handbook,* Vol. 5, Interscience, New York, 1975.
15. C. G. Vonk, *J. Appl. Crystallogr.,* **8,** 340 (1975).
16. L. E. Alexander, *X Ray Diffraction in Polymer Science,* Wiley, New York, 1969.
17. R. Fayt, R. Jerome, and Ph. Teyssie', *J. Polym. Sci., Polym. Phys. Ed.,* **20,** 2209 (1982).
18. R. Fayt, R. Jerome, and Ph. Teyssie', *J. Polym. Sci., Polym. Phys. Ed.,* **27,** 775 (1989).
19. R. Fayt, R. Jerome, and Ph. Teyssie', *Makromol. Chem.,* **187,** 837 (1986).